Interface magnetism in $Fe_2O_3/FeTiO_3$ heterostructures

Rossitza Pentcheva* and Hasan Sadat Nabi
Department of Earth and Environmental Sciences, University of Munich, Theresienstrasse 41, 80333 Munich, Germany
(Received 10 April 2008; published 15 May 2008)

To resolve the microscopic origin of magnetism in the $Fe_2O_3/FeTiO_3$ system, we have performed density functional theory calculations that take into account on-site Coulomb repulsion. By systematically varying the concentration, distribution, and charge state of Ti in a hematite host, we compile a phase diagram of the stability with respect to the end members and find a clear preference to form layered arrangements as opposed to solid solutions. The charge mismatch at the interface is accommodated through Ti^{4+} and a disproportionation in the Fe contact layer into Fe^{2+}, Fe^{3+}, leading to uncompensated moments in the contact layer and giving first theoretical evidence for the *lamellar magnetism hypothesis*. This interface magnetism is associated with impurity levels in the band gap, showing a half-metallic behavior and making $Fe_2O_3/FeTiO_3$-heterostructures prospective materials for spintronics applications.

DOI: 10.1103/PhysRevB.77.172405 PACS number(s): 75.70.Cn, 73.20.Hb, 71.28.+d

A challenge of today's materials science is to design ferromagnetic semiconductors that operate at room temperature (RT) for spintronics devices. Most of the efforts concentrate on homogeneous doping of semiconductors with magnetic impurities,[1–4] but the interfaces in complex oxides prove to be another source of a novel behavior.[5–7] The unique magnetic properties of the hematite-ilmenite system[8–10] (a canted antiferromagnet and a RT paramagnet, respectively) currently receive revived interest as a possible cause of magnetic anomalies in Earth's deep crust and on other planets[11] as well as for future device applications.[3,12,13]

Both hematite [a=5.035 Å, c=13.751 Å (Ref. 14)] and ilmenite [a=5.177 Å, c=14.265 Å (Ref. 15)] crystallize in a corundum(-derived) structure, which is shown in Fig. 1, wherein the oxygen ions form a distorted hexagonal close packed lattice and the cations occupy 2/3 of the octahedral sites. In α-Fe_2O_3 (space group $R\bar{3}c$), there is a natural modulation of electronic density along the [0001] direction wherein negatively charged $3O^{2-}$ layers alternate with positively charged $2Fe^{3+}$ layers. At RT, the magnetic moments of subsequent iron layers couple antiferromagnetically (AFM) in-plane with a small spin canting, which is attributed to spin-orbit coupling.[16–18] In ilmenite $FeTiO_3$, Fe and Ti layers alternate, which reduces the symmetry to $R\bar{3}$, and the corresponding sequence is $3O^{2-}/2Fe^{2+}/3O^{2-}/2Ti^{4+}$ with AFM coupling between the Fe layers and T_N=56–59 K.[19]

At the interfaces (IFs) in hematite-ilmenite exsolutions, the charge neutrality is disrupted. One way to balance the excess charge at the interface is by a disproportionation in the Fe layer, which now becomes mixed Fe^{2+} and Fe^{3+}. This *lamellar magnetism hypothesis (LMH)* was proposed by Robinson *et al.*[20] based on bond valence models and kinetic Monte Carlo (kMC) simulations with empirical chemical and magnetic interaction parameters. The increased technological interest in this system calls for an atomistic material specific understanding that can only be obtained from first principles calculations. A previous density functional theory (DFT) study within the generalized gradient approximation (GGA) found no evidence for the LMH.[21] However, electronic correlations, which are not included in the local (spin-) density approximation (LSDA) or the GGA of the DFT, play an important role in transition metal oxides. Such effects were recently considered within LSDA+U[22] or by using hybrid functionals[23] for single Ti impurities in hematite; however, layered arrangements and interfaces were not addressed.

In this Brief Report, we have performed DFT calculations including a Hubbard U[24] for the end members Fe_2O_3 and $FeTiO_3$, as well as their interfaces and solid solutions (SS). By systematically varying the concentration, distribution, and charge state of Ti incorporated in a α-Fe_2O_3 host, we explore different scenarios for the charge compensation mechanism and its consequences for the magnetic and electronic behavior. Finally, we compile a phase diagram of the stability of the different configurations with respect to the end members as a function of Ti doping by also taking the effect of strain into account.

Our DFT-GGA[25] calculations are performed by using the all-electron full-potential augmented plane waves method, as

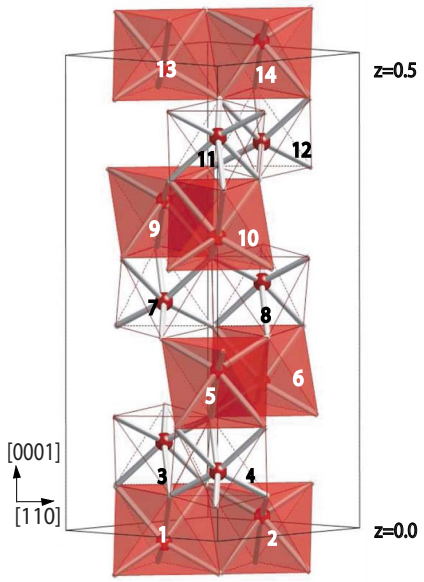

FIG. 1. (Color online) Crystal structure of $FeTiO_3$ showing half of the 60-atom unit cell. The cation sites are numbered and oxygen occupies the edges of the octahedra.

TABLE I. Relative stability (eV/60-atom cell) of the different cation arrangements in the Ti^{4+}, Fe^{2+}, Fe^{3+} charge state (strained at the Fe_2O_3 lattice parameters) with respect to the most stable configuration, whose energy is set to 0.0 eV. The positions occupied by Ti are denoted as subscripts according to Fig. 1 (SSL: spin sublattice). The total magnetic moment, electronic behavior (hm and m denote half-metallic and metallic, respectively), as well as the Ti^{4+}-O and Fe^{2+}-O distances at the interface are also displayed.

System	ΔE (eV)	$d_{Ti^{4+}-O}$ Å	$d_{Fe^{2+}-O}$ Å	M_{tot} (μ_B)	Δ (eV)
		Ilm_{17}			
$T_{1,2}$: 1 Ti layer	0.0	1.90	2.08	−8.0	hm
T_7: single impurity	0.20	1.93	2.02	12.0	hm
		Ilm_{33}			
$T_{1,2,13,14}$: 1 Ti layer	0.36	1.90	2.08	−16.0	hm
$T_{3,4}$: 2 Ti layers	0.00	1.89	2.08	16.0	hm
$T_{5,10}$: same SSL	0.19	1.86	2.04	−16.0	hm
$T_{5,7}$: different SSL	0.41	1.92	2.02	0.0	m
$T_{5,8}$: different SSL	1.24	1.86	2.06	0.0	hm
		Ilm_{50}			
$T_{1,2,5,6}$: 3 Ti layers	0.00	1.90	2.07	−24.0	hm
$T_{3,4,7}$: Ti-Fe@IF	1.23	1.96	2.00	8.0	hm
		Ilm_{66}			
$T_{3,4,11,12}$: 4 Ti layers	0.00	1.90	2.07	16.0	hm
$T_{3,6,9,12}$: SS	0.95	1.92	2.02	0.0	hm

implemented in WIEN2K.[26] Electronic correlations are considered within the fully localized limit (LDA+U).[24] The systems are modeled in the hexagonal primitive unit cell (shown in Fig. 1) containing 30 and 60 atoms. For these, 24 and 15 k points in the irreducible part of the Brillouin zone were used, respectively. Inside the muffin tins ($R_{MT}^{Fe,Ti}$ =1.80 bohr, R_{MT}^{O}=1.60 bohr) wave functions are expanded in spherical harmonics up to l_{max}^{wf}=10 and nonspherical contributions to the electron density and potential up to $l_{max}^{pot.}$=6 are used. The energy cutoff for the plane wave representation in the interstitial is E_{max}^{wf}=19 Ry for the wave functions and $E_{max}^{pot.}$=196 Ry for the potential. These convergence parameters ensure a numerical accuracy of energy differences better than 0.01 eV/60-atom cell. A full structural optimization of internal parameters within GGA+U[27] has been performed.

As a starting point, we have modeled the end members Fe_2O_3 and $FeTiO_3$. In agreement with previous calculations,[22,28] GGA+U considerably improves the band gap of hematite from 0.43 eV (GGA) to 2.2 eV for U =6 eV and J=1 eV in close agreement with measured values of 2.14–2.36 eV.[29,30] Also, the type of band gap changes from a Mott–Hubbard between Fe3d-Fe3d states to charge transfer after the scheme of Zaanen *et al.*[31] between occupied O 2p and empty Fe 3d states.

For ilmenite, the GGA incorrectly predicts a metallic state;[32] hence, the inclusion of Hubbard U (U=8 eV, J =1 eV) is decisive to obtain a Mott–Hubbard gap of 2.18 eV (Δ^{exp}=2.54 eV[9]) between the occupied Fe d_{z^2} orbital and the unoccupied Fe 3d states in one spin channel (all Fe 3d orbitals being occupied in the other spin channel). These U and J values are used both on Fe and Ti in the following: A Fe^{3+}/Ti^{3+} charge arrangement lies 0.63 eV/p.f.u. above the ground state Fe^{2+}/Ti^{4+}. For $Fe^{2+}Ti^{4+}O_3$, the AFM and FM couplings between Fe layers are nearly degenerate, which is consistent with the low T_N.

In the following, we vary the concentration and distribution of Ti in a Fe_2O_3 host. The positions of the Ti ions are given as subscripts and follow the notation in Fig. 1, e.g., $T_{3,4,7,8,11,12}$ describes pure ilmenite. Table I contains the energetic stability, structural, magnetic, and electronic properties of different cation arrangements and concentrations. We start the discussion with Ilm_{33}, which corresponds to four Ti ions out of 24 cations in the 60-atom cell. We find that the formation of a compact ilmenite-like block with a Fe layer sandwiched between two Ti layers ($T_{3,4}$) is 0.36 eV more favorable than the incorporation of the single Ti layers in the hematite host ($T_{1,2,13,14}$). The spin density of $T_{3,4}$ plotted in Fig. 2(a) shows that the central Fe layer turns into Fe^{2+} and the charge mismatch at the IF is compensated by Fe^{2+}, Fe^{3+} in the contact layer, which gives theoretical evidence from first principles for the lamellar magnetism hypothesis of Robinson *et al.*[20] Our GGA+U calculations show that Ti_4^{4+} shares faces with Fe_5^{3+}, while Fe_6^{2+} shares faces with Fe_8^{3+} from the next hematite layer. Such a configuration was proposed by using bond-valence sums[33] and kMC simulations[34] only after considering both chemical and magnetic interactions.

The formation of layered arrangements ($T_{3,4}$) is favored compared to a more random distributions with 50% substituted cation layers (e.g., $T_{5,10}$, $T_{5,7}$, or $T_{5,8}$). With respect to magnetism, each Ti ion adds a magnetic moment of $4\mu_B$ independent of whether the extra electron is localized at Ti (Ti^{3+}) or at a neighboring Fe (Fe^{2+}). In solid solutions, the total magnetic moment depends on the site and sublattice

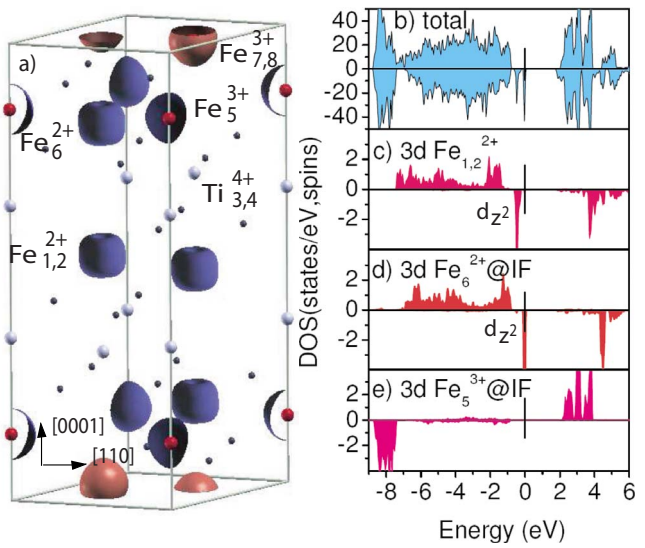

FIG. 2. (Color online) (a) Spin density distribution and [(b)–(e)] total and projected density of states of Ti double layer in hematite ($T_{3,4}$) with $Fe^{2+}_{1,2}$, $Ti^{4+}_{3,4}$ and a disproportionated Fe^{3+}_{5}, Fe^{2+}_{6} layer at the interface. The position of the Fermi level is set to 0.0 eV and denoted by a short line. In (a), positions of Ti, Fe, and O are marked by the light gray, red (dark gray), and small black circles, respectively.

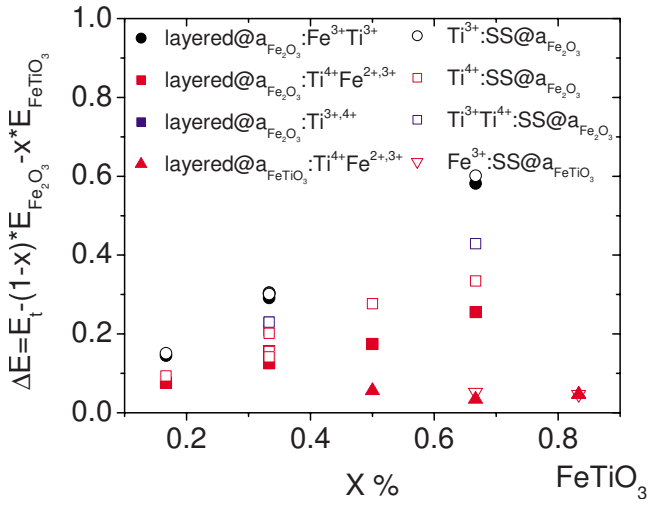

FIG. 3. (Color online) Formation energy (eV/p.f.u) with respect to the end members as a function of ilmenite concentration x. Layered arrangements (solid solutions) are denoted by the full (open) symbols.

where Ti is built in. We find that incorporation in the same spin-sublattice $T_{5,10}$ (which maximizes the magnetic moment) is favored by 0.22 eV compared to the AFM $T_{5,7}$. Taking local lattice relaxations into account enhances the energy gain compared to previous calculations by Velev *et al.*[22] (0.08 eV). Still, some degree of Ti disorder is likely in quickly cooled samples, which reduces the expected magnetization as observed by Chambers *et al.*[3] ($0.5 \pm 0.15 \mu_B$/Ti for $x_{Ti}=0.15$). For higher Ti concentrations and longer annealing steps, the formation of the thermodynamically more stable layered ferrimagnetic phase is expected, which is consistent with the strong correlation between cation order and ferrimagnetism found in annealed samples[8,12] and the saturation magnetization of $3\mu_B$/mol measured in epitaxial films with $x_{Ti} \leq 0.63$.[13] Below the ordering temperature of ilmenite, only ilmenite lamella with an odd number of Ti layers are expected to carry a nonzero magnetization, whereas, above 56 K, the net magnetic moment will be solely due to the uncompensated magnetic moments in the contact layers, which is independent of the number of Ti layers within the paramagnetic ilmenite lamella.

Concerning the electronic properties, doping Fe_2O_3 with Ti leads to impurity levels in the band gap arising from the occupied d_{z^2} orbital of Fe^{2+} ions in the contact layer. The density of states plotted in Fig. 2(d) shows that these states are pinned at the Fermi level, which leads to fully spin-polarized carriers and half-metallic behavior for $T_{3,4}$. This trend is robust with respect to U (Ref. 35) and is observed for most of the studied cation concentrations and arrangements after structural relaxation. Experimentally, a semiconducting behavior and a drop in resistivity of several orders with respect to the end members is measured.[3,9,12,13] The measured values suggest localized rather than itinerant carriers consistent with the picture, we obtain from LDA+U.

Next, we turn to the energetic stability as a function of the Ti concentration displayed in Table I and the phase diagram in Fig. 3. Charge compensation through Ti^{4+} and disproportionation of iron into Fe^{2+}, Fe^{3+} is strongly favored compared to compensation involving Ti^{3+}, especially after optimization of the internal structural parameters. Moreover, the formation of layered configurations (full symbols) is preferred over disordered arrangements (empty symbols) except for very high (>83%) and very low concentrations (<17%), which is consistent with the miscibility gap from thermodynamic data (e.g., Refs. 21 and 36). The linear increase in formation energy in the range between Ilm_{17} and Ilm_{66} indicates that straining Ti doped Fe_2O_3 to the Fe_2O_3 lattice parameters gets increasingly unfavorable with growing x. On the other hand, using the ilmenite lattice parameters at $x=66\%$ instead of hematite (volume increase of 8.7%) leads to an energy gain of 0.22 eV/p.f.u. for $T_{7,8,11,12}$ (red filled up triangles in Fig. 3).

An interesting trend is observed in the shortest cation-oxygen bond lengths (cf. Table I), which tend to relax toward the values in the respective end member. While $d_{Fe^{3+}-O}$ (not shown) remains close to the value in bulk hematite (1.96 Å), the bond lengths of the Ti impurity and the neighboring Fe^{2+} relax toward the values in bulk ilmenite (1.92 and 2.07 Å, respectively).

In Fe doped ilmenite, the trend toward layered arrangements is retained for 66%, e.g., $T_{7,8,11,12}$ is favored by 0.21 eV compared to $T_{3,8,11,12}$, but ordered and disordered phases are nearly degenerate at 83%. Fe substituting for Ti in the ilmenite lattice is Fe^{3+}. Additionally, one Fe in the neighboring layer turns Fe^{3+} to compensate the charge, which forms a Fe^{2+}, Fe^{3+} contact layer. The substituted Fe shows a strong tendency to couple antiparallel to the neighboring Fe layers.

In summary, we present a comprehensive GGA+U study of the cation, charge, and magnetic order in the hematite-ilmenite system, which shows a strong preference toward

formation of layered configurations as opposed to solid solutions. At the interface between hematite and ilmenite blocks, we find evidence for the lamellar magnetism hypothesis[20] with a disproportionated Fe^{2+}, Fe^{3+} contact layer to accommodate the polar discontinuity. These uncompensated moments lead to the ferrimagnetic behavior of the system. The d_{z^2} orbital in one spin channel (all d orbitals being occupied in the other) at the Fe^{2+} sites in the contact layer crosses the Fermi level leading to half-metallic behavior in most of the studied compositions. The ferrimagnetism emerging at the interface of two antiferromagnetic oxides such as hematite and ilmenite is an impressive example of the novel functionality that can arise as a consequence of a polar discontinuity and the richer possibilities to compensate it that complex oxides offer.[37,38] Recently, an exchange bias of more than 1 T was reported in this system.[39] Further phenomena such as oscillatory exchange coupling and spin-polarized transport remain to be explored in controlled epitaxial Fe_2O_3-$FeTiO_3$ multilayers on the route to possible device applications.

We gratefully acknowledge discussions with M. Winklhofer, W. Moritz, R. Harrison, P. Robinson, and S. McEnroe as well as funding by the DFG (Grant No. Pe883/4-1) and ESF within the European Mineral Science Initiative (EuroMinSci). Simulations were performed on the high performance supercomputer at the Leibniz Rechenzentrum.

*pentcheva@lrz.uni-muenchen.de

[1] J. M. D. Coey, M. Venkatesan, and C. B. Fitzgerald, Nat. Mater. **4**, 173 (2005).
[2] A. H. MacDonald, P. Schiffer, and N. Samarth, Nat. Mater. **4**, 195 (2005).
[3] S. A. Chambers *et al.*, Mater. Today **9**, 28 (2006).
[4] S. Kuroda *et al.*, Nat. Mater. **6**, 440 (2007).
[5] A. Ohtomo *et al.*, Nature (London) **419**, 378 (2002).
[6] A. Brinkman *et al.*, Nat. Mater. **6**, 493 (2007).
[7] N. Reyren *et al.*, Science **317**, 1196 (2007).
[8] Y. Ishikawa and S. Akimoto, J. Phys. Soc. Jpn. **12**, 1083 (1957).
[9] Y. Ishikawa, J. Phys. Soc. Jpn. **13**, 37 (1958).
[10] C. M. Carmichael, Proc. R. Soc. London, Ser. A **263**, 508 (1961).
[11] T. Kasama *et al.*, Earth Planet. Sci. Lett. **224**, 461 (2004).
[12] Y. Takada *et al.*, J. Magn. Magn. Mater. **310**, 2108 (2007).
[13] H. Hojo *et al.*, Appl. Phys. Lett. **89**, 142503 (2006).
[14] D. A. Perkins and J. P. Attfield, J. Chem. Soc., Chem. Commun. **4**, 229 (1991).
[15] R. J. Harrison, S. A. T. Redefern, and R. I. Smith, Am. Mineral. **85**, 194 (2000).
[16] L. M. Sandratskii and J. Kübler, Europhys. Lett. **33**, 447 (1996).
[17] I. J. Dzyaloshinsky, Phys. Chem. Solids **4**, 241 (1958).
[18] T. Moriya, Phys. Rev. **120**, 91 (1960).
[19] P. F. McDonald *et al.*, J. Appl. Phys. **69**, 1104 (1991).
[20] P. Robinson *et al.*, Nature (London) **418**, 517 (2002).
[21] B. P. Burton, A. Chaka, and D. J. Singh, Phase Transitions **78**, 239 (2005).
[22] J. Velev, A. Bandyopadhyay, W. H. Butler, and S. Sarker, Phys. Rev. B **71**, 205208 (2005).
[23] T. Droubay, K. M. Rosso, S. M. Heald, D. E. McCready, C. M. Wang, and S. A. Chambers, Phys. Rev. B **75**, 104412 (2007).
[24] V. I. Anisimov, I. V. Solovyev, M. A. Korotin, M. T. Czyzyk, and G. A. Sawatzky, Phys. Rev. B **48**, 16929 (1993).
[25] J. P. Perdew, K. Burke, and M. Ernzerhof, Phys. Rev. Lett. **77**, 3865 (1996).
[26] P. Blaha, K. Schwarz, G. K. H. Madsen, D. Kvasnicka, and J. Luitz, WIEN2k, An Augmented Plane Wave+Local Orbitals Program for Calculating Crystal Properties (Technical University Wien, Austria, 2001), ISBN3-9501031-1-2.
[27] F. Tran, J. Kunes, P. Novak, P. Blaha, and L. D. Marks (unpublished).
[28] G. Rollmann, A. Rohrbach, P. Entel, and J. Hafner, Phys. Rev. B **69**, 165107 (2004).
[29] D. Benjelloun *et al.*, Mater. Chem. Phys. **10**, 503 (1984).
[30] R. H. Chang and J. B. Wagner, J. Am. Ceram. Soc. **55**, 211 (1972).
[31] J. Zaanen, G. A. Sawatzky, and J. W. Allen, Phys. Rev. Lett. **55**, 418 (1985).
[32] N. C. Wilson, J. Muscat, D. Mkhonto, P. E. Ngoepe, and N. M. Harrison, Phys. Rev. B **71**, 075202 (2005).
[33] P. Robinson, R. J. Harrison, and S. A. McEnroe, Am. Mineral. **91**, 67 (2006).
[34] R. J. Harrison, Am. Mineral. **91**, 1006 (2006).
[35] The same half-metallic behavior is also obtained for a lower U value of 6 eV.
[36] S. A. McEnroe *et al.*, Geophys. J. Int. **151**, 890 (2002).
[37] R. Pentcheva and W. E. Pickett, Phys. Rev. B **74**, 035112 (2006).
[38] R. Pentcheva and W. E. Pickett, Phys. Rev. Lett. **99**, 016802 (2007).
[39] S. A. McEnroe *et al.*, Nat. Nanotechnol. **2**, 631 (2007).